We are IntechOpen, the world's leading publisher of Open Access books Built by scientists, for scientists

4,800
Open access books available

122,000
International authors and editors

135M
Downloads

Our authors are among the

154
Countries delivered to

TOP 1%
most cited scientists

12.2%
Contributors from top 500 universities

CLARIVATE ANALYTICS BOOK CITATION INDEX INDEXED

WEB OF SCIENCE™

Selection of our books indexed in the Book Citation Index in Web of Science™ Core Collection (BKCI)

Interested in publishing with us?
Contact book.department@intechopen.com

Numbers displayed above are based on latest data collected.
For more information visit www.intechopen.com

28

Surface Acoustic Waves and Nano–Electromechanical Systems

Dustin J. Kreft and Robert H. Blick
University of Wisconsin – Madison
Department of Electrical and Computer Engineering
U.S.A.

1. Introduction

Surface acoustic waves (SAW) follow the industrial trend of reducing the size, enhancing the speed, while enhancing the efficiency of energy coupling. Integrating this with micro-electromechanical systems (MEMS) and nano-electromechanical systems (NEMS) offers a wide variety of applications such as touch screens, gas and biological sensors, and embedded RFID devices. With modern lithographic techniques, allowing the fabrication of smaller SAW devices, we now use SAWs to probe the mechanical interactions of nano structures. In particular, SAWs can be used to actuate NEMS which gives rise to many interesting phenomena including anomalous acoustoelectric currents, shock waves in suspended devices, and few electron transport, to only name a few, (Beil et al., 2008; Talyanskii et al., 1997). Today, SAWs are also used to generate a quantized current for use as a current standard. In practice two counter-propagating SAWs are used to observe a quantized acoustoelectric current. This leads to population and depopulation of discrete states (Kataoka et al., 2007). In the following we want to give an overview of the state of the art of applying SAWs to nanomechanical devices. We will also give a brief introduction to recent nanoelectromechanical systems with integrated low-dimensional electron gases, which have the potential to reveal insights into quantized acoustoelectric states.

2. Fabrication

The focus for generating SAWs in this chapter will involve the fabrication of interdigitated transducers (IDT). An IDT is simple in concept but can be very involved when fine tuning a structure for engineering applications. Such topics as electronic impedance matching to RF lines, effects of bulk waves in contrast to SAWs, and increasing bandwidth will not be covered; though, this is simply a shortened list of things to consider when designing a proper IDT for engineering applications, they do fall outside the scope of this chapter. Nevertheless, another fabrication step we will consider is the use of acoustic waveguides for acoustic impedance matching of IDTs to nanomechanical devices.

2.1 Interdigitated Transducer Design

The main equation to consider when designing an IDT is:

$$v = \lambda f \tag{1}$$

Where v is the velocity of sound in the material, λ is the SAW wavelength or pitch of the IDT, and f is the frequency of the propagating SAW. The pitch of the IDT fingers is the same as the SAW wavelength, λ, which will propagate across the sample. Fig. 1 shows a simple IDT schematic along with a scanning electron micrograph (SEM) image and optical image.

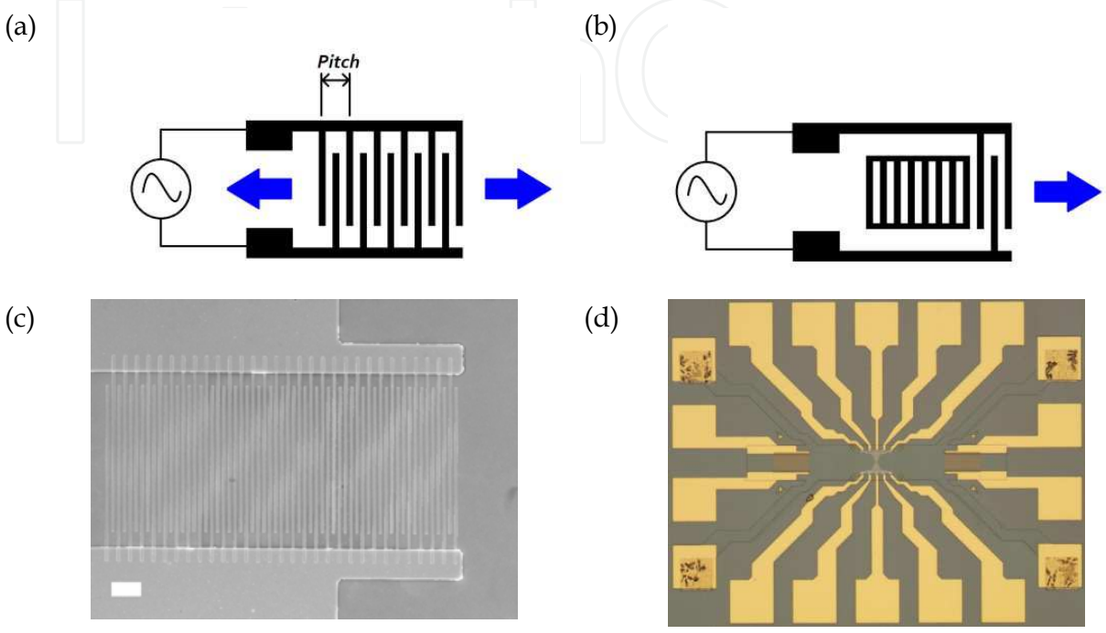

Fig. 1. Schematics and scanning electron microscope images of IDTs. (a) Schematic of bidirectional IDT, (b) schematic of unidirectional IDT through the use of a reflection grating, (c) SEM image of a bidirectional IDT on GaAs with a pitch of 4 μm and a center frequency of ~715 MHz. The scale bar is 10 μm. (d) Optical image of device with an IDT on both ends and a nanomechanical device placed in the center

In Fig. 1 the arrows indicate the SAW propagation directions. It can be easily seen that the SAW will propagate in both directions away from the IDT. A singly propagating SAW direction can be achieved by placing a reflection grating on one end of the SAW. The reflection grating will have the same geometry as the IDT; that is, the same finger spacing and width. The grating distance from the IDT is ~ $\lambda/2$. The IDT fingers are typically chosen with evenly spaced fingers, where the spacing between the fingers is equal to the finger width. The finger width and finger spacing is $\lambda/4$ in this scenario and gives a metallization ratio of $\eta = 0.5$, which will generate only odd harmonics with no response of the third harmonic (Campbell, 1998). The bandwidth of an IDT is defined as $BW\% = f / N_{Pairs}$. Where f, again, is the center frequency and N_{Pairs} is the number of finger pairs of the IDT. The IDT in Fig. 1a has five pairs of fingers and is symmetric about a center point along the axis of SAW propagation. It is typical to fabricate two IDTs, one on each end of the device, so that their propagating waves can interfere either constructively or destructively across the center region of the device; this is typically the region where a Quantum Point Contact (QPC) or other structures resides. This can be seen in Fig. 1d where in the center a double quantum dot (DQD) is placed and the IDTs are placed to the left and right.

2.2 Acoustic Waveguide Design

Another detail of fabrication is the use of waveguides for the SAW. A waveguide for SAWs is a pattern that is fabricated onto the device so the SAWs can be guided into a certain region allowing a stronger SAW signal or amplitude; it is analogous to a coplanar waveguide for RF signals. When fabricating IDTs, and a device as a whole, using waveguides does not have much of a use in the areas of RFID, cellular delay lines, sensors, and other non-region specific devices. However, this chapter will focus on NEMS and the use of SAWs to interact with these devices. Since the NEMS device is orders of magnitude smaller than the IDT aperture very little SAW power can interact with the NEMS structure; it can be beneficial to include a waveguide to focus the SAW onto the nanostructure.

Waveguides can be modeled using standard acoustic, or horn, waveguides with some minor tuning. There are several shapes which can be used and each shape offers its own benefits regarding a particular application. We will start by first mentioning the base equation for hyperbolic horns used in speaker systems, these horns can also be referred to as hyperbolic-exponential horns or hypex horns (Salmon, 1946).

$$A = A_t[\mathrm{Cosh}(kx) + T \cdot \mathrm{Sinh}(kx)]^2 \tag{2}$$

$$z = \frac{\rho_0 v}{A_t}\left(\sqrt{1 - \left(\frac{f_c}{f}\right)^2} + i\frac{f_c T}{f}\right)\left(1 - \frac{f_c^2(1 - T^2)}{f^2}\right)^{-1} \tag{3}$$

Eq. 2 gives the wave front area expansion of the wave as propagating through the waveguide or horn. A_t is the area of the throat, or base, of the waveguide, T is a factor describing the shape of waveguide; for T = 1 the waveguide becomes exponential in shape, and becomes canonical as $T \to \infty$, k is given as $(2\pi f_c)/v$; where v is the velocity of sound, and f_c is the cutoff frequency of the waveguide. For hyperbolic and exponential waveguides there is no transmission below the cutoff frequency, f_c, since at this point the impedance is purely reactive. Eq. 3 gives the impedance of the waveguide; all variables are defined previously with the addition of ρ_0 which is the density of the material.

Fig. 2 contains three SEM images of an exponential waveguide with a tube waveguide in the center. A tube waveguide is simply a small or narrow SAW delay line. The material is a GaAs/AlGaAs heterostructure containing a two-dimensional electron gas (2DEG) and a sacrificial layer. We use a 2DEG because the high electron mobility makes this an ideal candidate for nanostructures, such as quantum dot (QD) and DQD systems. The waveguide was defined using electron-beam lithography to open up an etch region through the PMMA. The material was then wet etched with H_3PO_4:H_2O_2:H_20 into the sacrificial layer. Then diluted HCl was used to remove the sacrificial layer which resulted in a suspended region in the center and around the waveguide. This suspended region is visible as a darkened shadow indicating a height difference due to strain relaxation of the material. The suspended region forms the actual nanomechanical device. Since this device contains a DQD in the center region of the structure it is beneficial to use a waveguide to ensure a higher SAW power density coupled into that region. Since the IDT aperture of this device is 50 μm and the DQD region is roughly 600 nm at the widest QPCs.

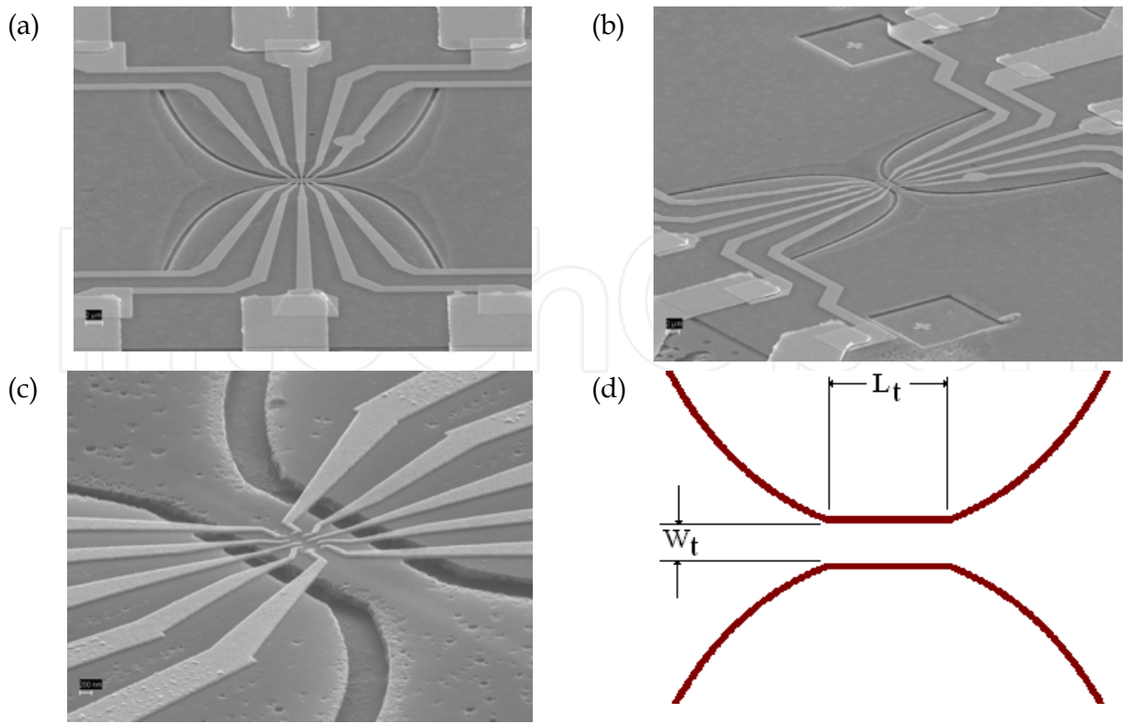

Fig. 2. SEM images of an exponential waveguide with a cutoff frequency of 75 MHz and throat width of ~1.5 μm. The darker region around the waveguide shows that the area is suspended, which was achieved by an HCl etch to remove the sacrificial layer below the 2DEG, (a), (b) and (c). (d) Schematic of waveguide, center region is the throat (pipe waveguide) with width W_t and length L_t. The outer curves are the exponential portion of the waveguide

3. Surface Acoustic Waves in Two Dimensional Electron Gases

3.1 Surface Acoustic Wave Basics

When applying an RF signal to the IDTs an alternating electric potential is seen by the electrodes, this will create an electric field distribution within the piezoelectric substrate, see Fig. 3a. This field distribution, in turn, will cause a mechanical deformation of the material through the inverse piezoelectric effect. As stated before, this mechanical deformation will propagate away from the IDTs and continue to move along the surface of the device, see Fig. 3d. Here we neglect other forms of waves being produced such as bulk waves.

Once the RF signal of the IDT is coupled into the piezoelectric substrate a Rayleigh-wave is produced. The elliptical wave propagating (Fig. 3b, d) along the surface can be described quite accurately by a traveling wave:

$$U = |U| e^{i(\omega t - kz)} e^{-k|y|} \tag{4}$$

The electric potential being created by the propagating wave can also be described in a like manner:

$$\Phi = |\Phi| e^{i(\omega t - kz)} e^{-k|y|} \tag{5}$$

In both Eqs. 4 and 5, ω is the angular frequency and k is the phase constant. The SAW penetrates into the depth of the material by about one wavelength, ~λ. This value is different in the suspended region. Hence, the actuation of nanomechanical resonators is considerably enhanced. Another property of the SAW is that the electric field created from the induced electric potential does not terminate at the surface of the material but can extend beyond by λ.

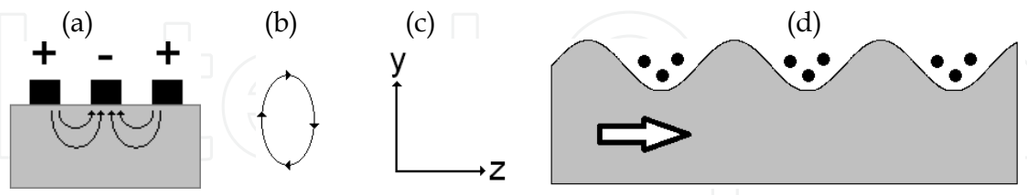

Fig. 3. (a) Side view of IDT with an applied voltage, the electric field couples into the piezoelectric substrate causing a deformation. (b) The elliptical motion of the Rayleigh-wave. (c) Axis used for reference in equations as it applies to the orientation of the piezoelectric substrate. (d) Side view of piezoelectric material as it is deformed causing a SAW to propagate

The set of base equations used for describing SAW phenomena are listed.

$$E_i = -\frac{\partial \Phi}{\partial x_i} \tag{6}$$

$$T_{ij} = c_{ijkl} S_{kl} + e_{nij} E_n \tag{7}$$

$$S_{kl} = \frac{1}{2}\frac{\partial u_k}{\partial x_l} + \frac{\partial u_l}{\partial x_k} \tag{8}$$

Eq. 6 is the electric field intensity that is produced from the deformed piezoelectric material from the SAW. Eq. 7 is the piezoelectric mechanical stress and Eq. 8 is the linear strain displacement.

3.1.1 Attenuation

SAW attenuation can be described by the following equations (Wixworth et al., 1989):

$$\Gamma = k\frac{K^2_{eff}}{2}\frac{\sigma_s / \sigma_M}{1+(\sigma_s / \sigma_M)^2} \tag{9}$$

$$\frac{\Delta v}{v} = k\frac{K^2_{eff}}{2}\frac{1}{1+(\sigma_s / \sigma_M)^2} \tag{10}$$

Here the attenuation occurs because part of the longitudinal electric field of the propagating wave couples into the electrons of the 2DEG. This not only causes a current to flow but pulls power from the SAW due to ohmic losses. This attenuation is described by Eq. 9. A SAW velocity shift is also observed due to the piezoelectric stiffening of the substrate, see Eq. 10 (Wixworth et al., 1989). Below are the recreated graphs from (Wixworth et al., 1989) to show the relationship of the attenuation and sound velocity shift due to a change in conductivity.

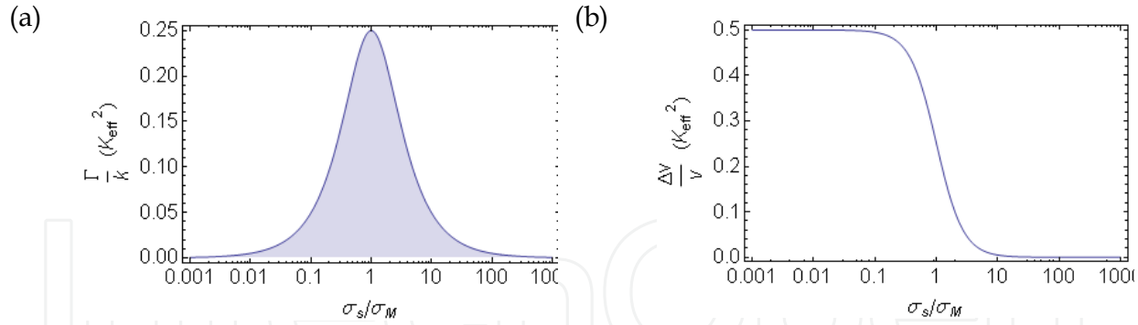

Fig. 4. (a) The SAW attenuation in units of K_{eff}^2, see Eq. 9. (b) The change in SAW velocity in units of K_{eff}^2, see Eq. 10

Where k is the SAW wave vector, K^2_{eff} is the effective piezoelectric coupling coefficient, σ_s is the 2DEG sheet conductivity, and $\sigma_M = v_0(\varepsilon_1 + \varepsilon_2)$. Again, where v_0 is the sound velocity and ε_1 and ε_2 are the dielectric constants of the piezoelectric substrate and half space above it.

3.2 Acoustoelectric Current

As the SAW propagates across the material it creates two types of currents, one is the normal acoustoelectric current and the other being the anomalous acoustoelectric current. The normal acoustoelectric current is created by electrons being "dragged" across the material and can be described by Eq. 11 where I is the current, n is the number of electrons, e is the charge of an electron, and f is the frequency of the SAW or RF signal to the IDT. This current always flows in the direction of the SAW and is produced as a DC current despite an oscillating RF signal being applied to the IDTs. Eq. 11 shows that at higher frequencies the normal acoustoelectric current becomes quantized.

$$I = nef \tag{11}$$

$$j(z) = \frac{a\omega}{2\pi} \int_0^{2\pi/\omega} \sigma_{zz}(z,t)E_z(z,t)dt \tag{12}$$

Once this deformation occurs the energy bands in the material bend as well causing the electrons to fall into the created quantum wells and are dragged along with the SAW, see Fig. 3d. As the frequency increases the wavelength, and pitch of the IDT, decreases causing fewer energy states to be available within the wells. This idea is also implemented to generate QDs within the SAW, (Barnes et al., 2000).

The anomalous acoustoelectric current is produced from the deformation of the material and flows as a DC current. The difference is that the anomalous current always flows in one direction regardless of which IDT, left or right, produced the SAW. The current is smaller than the normal acoustoelectric current and is detected by different methods. The anomalous acoustoelectric current can be obtained by sweeping the RF signal of the IDTs and typically appears at an off-center frequency. Since the normal acoustoelectric current is much smaller, the anomalous current can be more easily detected, as shown in Fig. 5b. One such method for direct detection of the anomalous acoustoelectric current is to apply an RF signal to both the left and right IDTs, while phase locking the two signals (Beil et al., 2008). By phase locking the IDT signals a standing SAW can be created. Thus, a surface deformation is produced without a net direction of propagation. As seen in Fig. 5a the phase

is shifted between the two IDTs as the current is measured. At a phase difference of 180° the current tends towards zero.

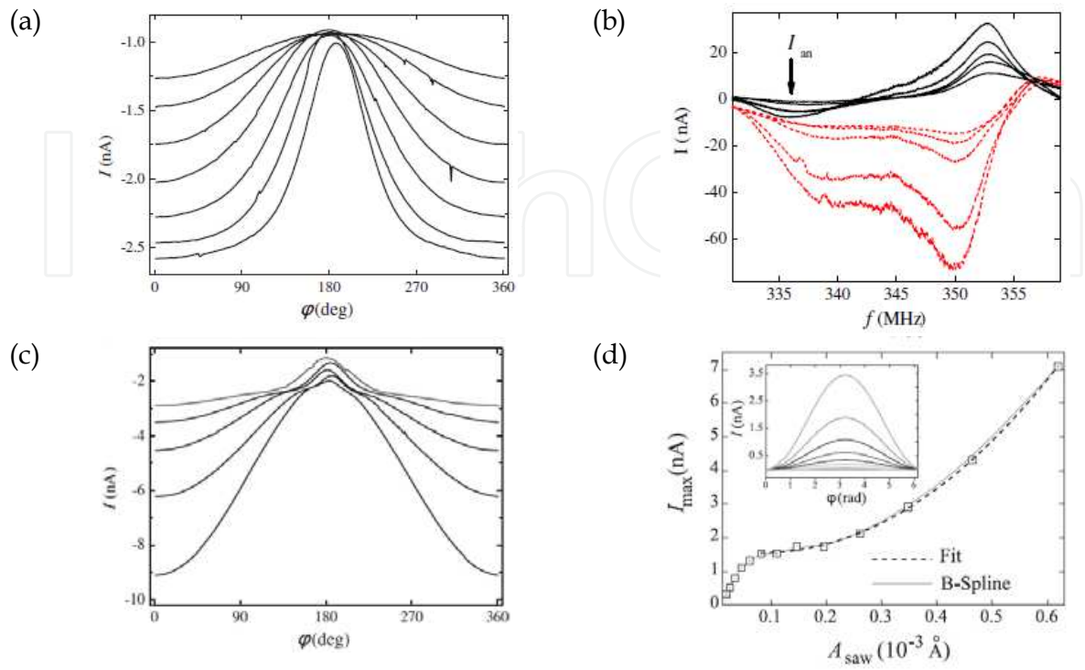

Fig. 5. Results for a suspended beam that is 1.2 µm long and 300 nm wide. (a) Anomalous acoustoelectric current as a result of phase adjusting two counter propagating SAWs. (b) Acoustoelectric current vs. applied frequency of the IDTs. There is always a negative current value to the left and is indicative of the anomalous current. (c) Formation of a shock wave seen by its Sinc(x) shape. The device's response jumps to a higher order mode and returns to Sin(x). (d) Derived anomalous acoustoelectric current amplitude as a result of the calculated SAW amplitude. All images are taken from Beil et al., 2008, Copyright (2008) by The American Physical Society

This zero current occurs because the two SAWs interfere destructively and create a nearly smooth surface with no deformation. At 0°, and also 360°, the current is at a maximum since the two SAWs interfere constructively allowing a maximum in the surface deformation.
The anomalous acoustoelectric current can be used to probe the SAW amplitude of a suspended beam or nanostructure. The accompanying graphs show the acoustoelectric current from the device. It has been shown that the anomalous acoustoelectric current through the device in relation to the SAW amplitude can be described by Eqs. 12-14; where Eq. 12 is the general equation for an anomalous acoustoelectric current, 13 is the derived equation, and 14 is the strain equation of the beam.

$$j_{an}(L/2) = -\frac{\sigma_0 e_{z4}}{2\varepsilon_{GaAs}}(\Pi_{zzzy} S_{zy}(L/2)^2) \tag{13}$$

$$S_{zy}(z,t) = 2A_t\left(\frac{6z^2}{L^3} - \frac{6z}{L^2}\right)\left(\mathrm{Cos}(\varphi/2) - \mathrm{Cos}(k_{SAW}L + \varphi/2)\right) \tag{14}$$

Where σ_0 is the unperturbed conductivity, ε_{GaAs} is the permittivity of GaAs, Π is a tensor which describes the effect of strain S, and A_t is the transverse component of the SAW.
An interesting phenomenon that occurs is the formation of shock waves in the suspended structure. From Figs. 5a and 5c it is seen that the device exhibits a Sin(x) type behavior in the anomalous acoustoelectric current at low RF powers. Once the RF power starts to increase it can be seen that the shape of the current starts to exhibit more of a Sinc(x) shape. This transition from a linear to a non-linear response indicates the formation of a shock wave in the suspended beam. As the power increases, the beam jumps into the next higher order mode and the current trace returns back to a linear response again. The shock wave formation is an indication that the beam will transition from one mode to another.

3.3 Surface Acoustic Waves in Magnetic Fields

We can use SAWs to probe the characteristics of a 2DEG under the presence of a magnetic field. Since a high mobility 2DEG is subject to Shubnikov-de Haas (SdH) oscillations, which creates changes in the conductivity, and SAWs are more sensitive to a conducting plane or surface, and the conductance of that plane, makes this combination an ideal candidate to investigate quantum effects of the 2DEG. The real interesting features are seen when integral Landau level filling factors are observed which causes a drop in conductivity of the 2DEG. At these quantized values the SAW responds strongly to the conductivity, σ.
In Fig. 6 it can be seen that the SdH oscillations and the acoustoelectric current oscillations are nearly identical. The SdH measurement was measured using a standard four-point lock-in technique, where as the acoustoelectric current was created by a SAW and was taken from two ohmic contacts on opposite sides of the sample. The peaks and valleys of the two measurements line up, for the most part, but there is a small offset. This offset is due to the fact that the SAW attenuation is not a linear with respect to the 2DEG conductivity, or magneto conductivity in this case, see Eq. 9.

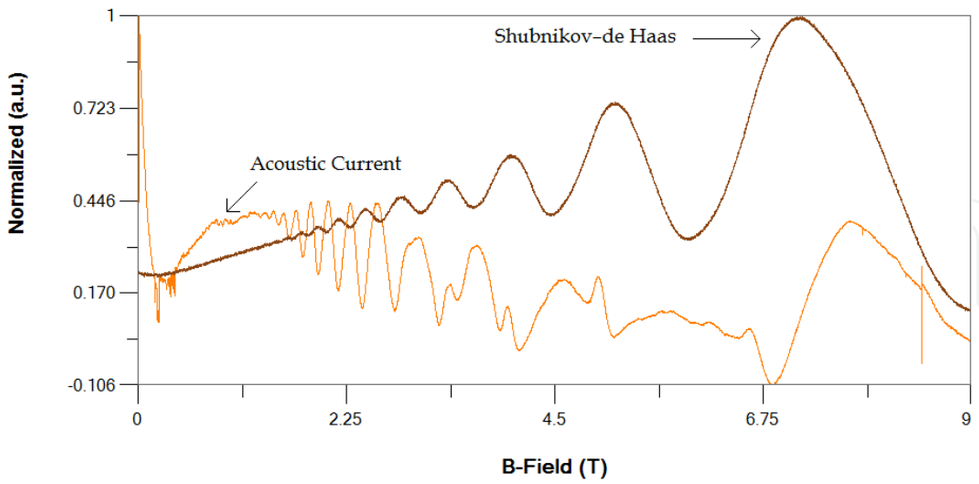

Fig. 6. A magnetic field, of maximum value 9 T, was applied perpendicular to the surface of the device. The device is shown in figures 1d and 2a-2d and contains a 2DEG 40 nm below the surface. Upper trace is the Shubnikov-de Haas oscillations measured using standard lock-in techniques and normalized to 713.4 Ω. The lower trace is the acoustoelectric current generated from a SAW with -12 dBm applied to the right IDT at 1.488 GHz and is normalized to 10.47 nA

Special attention has to be given to the acoustic current trace of Fig. 6 around 3 – 4 Tesla. There is a splitting of the peaks that occurs. This information does not appear in the SdH oscillation and is only isolated to a SAW effect. During this splitting the conductivity of the 2DEG is very low and σ_s becomes much smaller than σ_M, see Eq. 9. When this happens a maximum in SAW attenuation will occur which results in a reduced SAW amplitude. The center of a SAW current split is a minimum in the 2DEG conductivity; further details are discussed in Wixworth et al., 1989.

From Fig. 6 there are two observations that need to be explained. One is the spike-like feature or discontinuity around the 8.5 T mark of the acoustic trace. This is caused from SAW reflections on the sample. This spike-like feature can be seen on other data plots as well with SAW currents. The final feature is the negative acoustic current that was measured. Since at this point the SAW was highly attenuated, causing little or no current to flow, caused the sample itself to heat. The negative current may be a combination of a thermal current and a small offset in the measuring equipment.

4. Surface Acoustic Waves in Quantum Electronics

SAWs are used to produce a current in low dimensional electronic systems and NEMS. This can be used in various applications and for numerous different designs. The information presented in this section will deal with piezoelectric materials with an embedded two dimensional electron gas (2DEG); mainly GaAs/AlGaAs heterostructures unless otherwise stated. These measurements are carried out at liquid helium temperatures or lower, ≤ 4.2 K.

4.1 Quantum Point Contacts and Low Dimensional Channels

SAWs can be used to create a quantized current based upon Eq. 7. The advantage of the SAW inducing a quantized current is that this process can be used to populate and depopulate QDs and DQDs at higher frequencies then what can be used by applying an oscillating signal to the source-drain of the 2DEG. When using a SAW as the current source the acoustoelectric current can be pinched off in a Coulomb blockade just like a standard source-drain current can be. This pinch off is done via a quantum point contact (QPC) or a set of QPCs, which can be used to form QDs; see Fig. 7.

4.1.1 Quantum Point Contact Fabrication

Fabricating QPCs is done with the same methods as fabricating IDTs, see Sec. 2. Since QPCs are have small dimensions it is most common to use Electron Beam Lithography, or e-beam lithography, to create the structures. The exact dimensions of the QPC pair depends on what works best for the user and there is no set rules for design like there is for IDTs. When viewing Fig. 7 it can be seen that there are five sets of QPCs. A single QPC is seen as an electrode with another electrode opposite its position. All of the QPCs shown have a few common features; the tip of the QPC is small when compared to the rest of the electrode and the gap between the electrode tips is small as well. The tip is small so the electric field being emitted from the QPC is very localized, and the majority of the electrode is made wider so that it covers a wider portion of the 2DEG so the electrons are repelled. The gap between electrodes is small so pinch-off can be achieved with small voltages, more on this in Sec. 4.1.2.

4.1.2 Quantum Point Contact Operation

QPCs work by applying a negative voltage to them, this negative voltage produces an electric field that penetrates into the 2DEG causing electrons to be repelled at or around the QPC region; this can be seen if Fig 7(c). Here the black region represents the metallic electrode while the blue region represents the electric field and the green region represents the 2DEG or substrate. It can be taken as a good estimate that the electric field penetrates into the 2DEG from the QPC electrode at a 45° angle. As a larger negative voltage is applied to the QPC the effective screening electric field becomes larger causing the electron path within the 2DEG to become more constricted until single electron transport is achieved; this leads to a Coulomb Blockade, see Sec. 4.2. Then finally, the current is completely pinched off, see Figs 9 and 10.

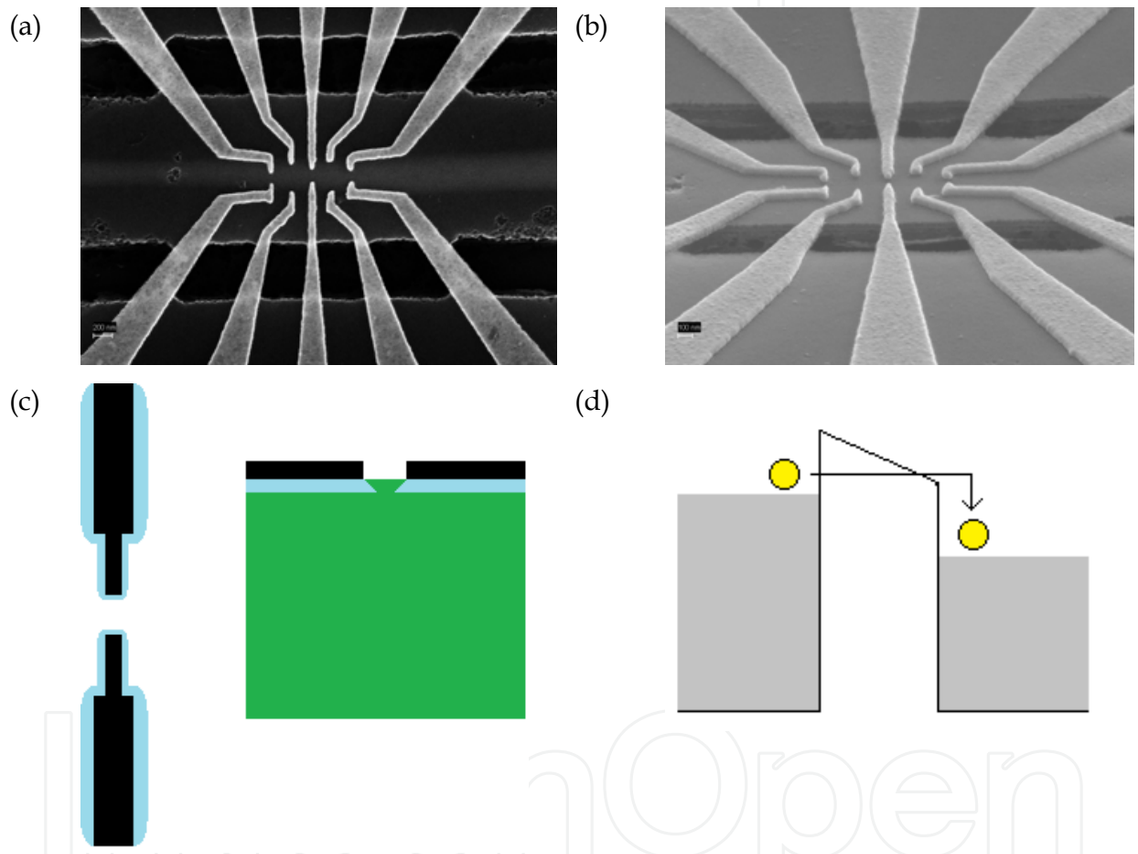

Fig. 7. Two SEM images of the same DQD structure on top of a suspended tube section of an acoustic waveguide. The DQD is made up of five pairs of QPCs. The material is a GaAs/AlGaAs heterostructure with an embedded 2DEG about 40 nm below the surface. (a) Top view with a scale bar of 200 nm, (b) angled view with a scale bar of 100 nm. (c) schematic view of QPC with applied voltage, the blue area represents the electric field surrounding the QPC and penetrating into the 2DEG (green). (d) Tunneling of electrons across potential barrier created by applied voltage from the QPC

The QPC creates a tunneling barrier which separates the source and drain regions of the sample. As the voltage magnitude becomes larger the strength, or height, or the tunneling barrier is increased and the width of the barrier becomes larger. When plotted a step like

feature can be seen which corresponds to a single conductance step which has a value of $G = 2e^2/h$, where h is Plank's constant and e is the charge of an electron. Now the temperature must be low so the thermal energy, $E = k_bT$, of the background is smaller than the tunneling energy needed for the electrons to "jump" across the barrier, where k_b is the Boltzmann constant. As seen in Figs 9 and 10 this step like feature can be seen by doing an I-V measurement. By changing the temperature of the system the phonon energy is increased and causes scattering events to increase, or increase the electron-phonon interaction, and the steepening or smoothing of the step like feature is a direct measure of this.

4.1.3 Usage of Quantum Point Contacts and Surface Acoustic Waves

The use of QPCs offers a benefit of determining which SAW mode(s) are propagating in the sample. Different SAW modes, such as bulk, longitudinal, and transverse with propagate at different frequencies due to the fact that they have different sound velocities, see Eq. 1. Another factor, which affects the sound velocity, is the propagation direction of the SAW with respect to the crystal orientation of the material. In Fig. 8 a QPC had an applied voltage of -0.8 V, which puts the QPC into pinch-off mode. Since it is in pinch-off higher RF power is required to create a sufficiently strong SAW that will overcome the potential barrier. As the power is increased from -18 dBm to -10 dBm, three peaks emerge as transferring current through the tunnel barrier. From Eq. 7 we can calculate the electron count to be 6, 3, and 2 for RF powers of -10 dBm, -12 dBm, and -14 dBm, respectively (some rounding is taken into account, due to thermal errors in measurement).

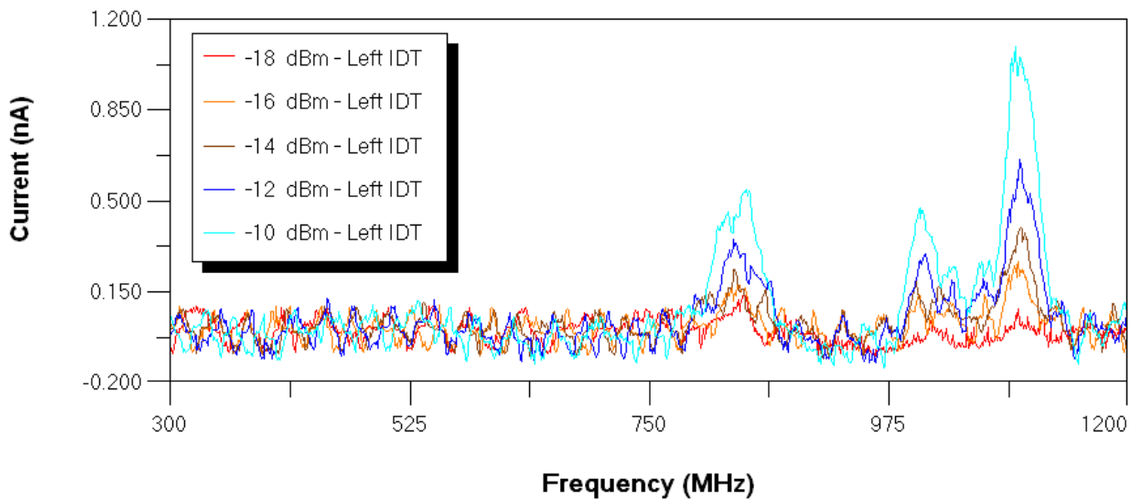

Fig. 8. A frequency sweep of varying RF powers while the center QPC of the sample in Fig. 4 is held at -0.8 V. The first peak is at 840 MHz with a current of 540 pA and a velocity of 3,368 m/s, the second peak at 1.005 GHz with a current of 472 pA and a velocity of 4,020 m/s, the third peak is at 1.095 GHz with a current of 1.098 nA and a velocity of 4,380 m/s

Now the three peaks represent different SAW modes. The highest frequency peak of Fig. 8 of 1.095 GHz represents a longitudinal wave with an acoustic velocity of 4,380 m/s and an angle of about 10^o off from the (110) direction (Kuok et al., 2001). This small angle variation is due to a small misalignment during the lithography process. When viewing the lower peak of 840 MHz at a velocity of 3,368 m/s, this coincides with a fast transverse wave with,

again, a 10° difference between the SAW direction and the (110) GaAs crystal orientation (Kuok et al., 2001).

4.2 Coulomb Blockade of Acoustoelectric Current

When looking over Fig. 9, we see that single steps are observed just before the total acoustoelectric current becomes zero. Focusing on Fig. 9a, we see that the last step is at about 0.5 nA. When solving with Eq. 11 the first step yields an answer of n = 1, i.e. a single electron is being transferred. We can look at all of the remaining steps and solve for them as well which will reveal integer numbers for n and will increase by 1 for each step, as is expected. Fig. 9a also shows that an applied voltage across the source and drain contacts, or ohmics, has very little effect on the final quantized acoustoelectric current. We do see, however, that a larger, or smaller, gate voltage is required for final pinch-off in the system but this is due to the small offset in the Fermi energy because of the applied bias. The only real difference is the shift from negative current to a positive current which is easy explained by the fact that the source-drain bias is producing a current that is opposite in direction, when $V_{ds} < 0$ mV, to that of the acoustoelectric current. Another aspect is the RF power dependence on the quantized current. When viewing Fig. 9b there is a similar trend to that of Fig. 9a. The small change in RF power has only a small effect on the acoustoelectric current. This is because the RF power is directly proportional to the SAW amplitude and we do not really identify any significant difference in the number of electrons being transferred, or Coulomb steps, until a drop of about 2 dBm.

So far an acoustoelectric current behaves in the same way as a standard source-drain bias current when a QPC is near pinch off. There is, however, another effect which can arise. As seen in Fig 9c a negative current arises and still exhibits the step like behavior. This negative current is the negative anomalous acoustoelectric current. This is said to be produced as an effect of SAW reflections, this is mostly seen in a two IDT system. The second IDT acts as a reflector much as the same way a reflection gradient is used for a unidirectional SAW, see Fig 1b. This can cause a standing wave to occur in the sample in such a way that the reflections effectively reduce the potential of the SAW and cause fewer electrons to be transported.

With slight phase shifts added the standing wave with respect to the QPC a net negative potential in the energy landscape can exist on one side of the QPC which will cause the current to change direction. These steps are best observed for QPCs that are long when compared to the SAW wavelength. This makes it possible to observe the acoustoelectric step current without applying a magnetic field (Shilton et al, 1996). As mentioned earlier, the high mobility of the 2DEG will screen the acoustoelectric current but this effect is not as prevalent when inside of a long QPC channel. The current screening is reduced around the QPC region and thus electrons can be transported through the channel. A long channel can allow ballistic transport of the electron causing it to shuttle from one side of the QPC to another. Since the screening is minimal, the electron will be "dragged" through the channel and the current steps of Fig. 9 can be observed.

Another phenomenon is oscillations in the acoustoelectric current once approaching the QPC pinch-off limit. As described in Shilton et al, 1996, and Maaø & Galperin, 1997, the acoustoelectric current oscillations occur at the same positions as the Coulomb steps. This oscillation is described as interference effects near the QPC at high frequencies which may be attributed to impurities in the 2DEG channel. The theory presented suggests that these

oscillations are due to state transitions, both propagating and reflecting (Maaø & Galperin, 1997). The SAW may reflect from the QPC and create interference patterns; these patterns will affect the electron transmission probability through the QPC simply by changing the potential landscape. This mechanism is also sensitive to scattering events near the QPC, where energy quanta are emitted and absorbed between two waves. Others have contributed to the theory and more is being added.

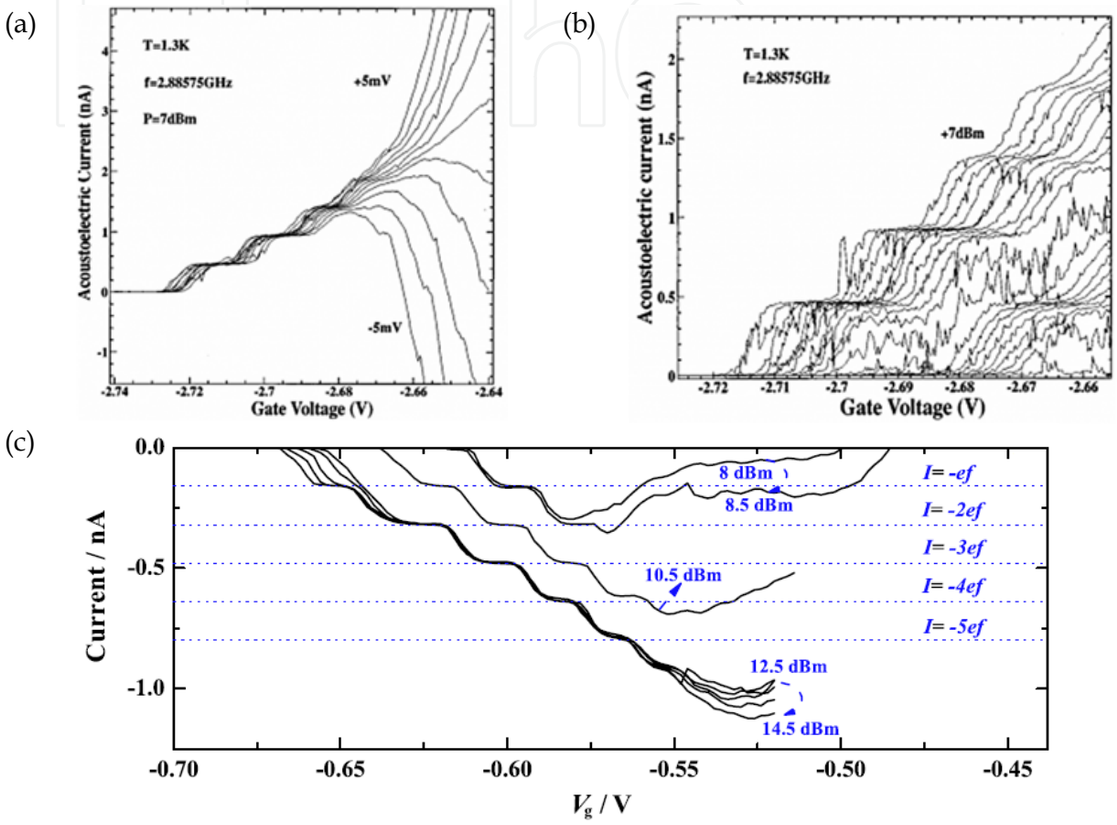

Fig. 9. QPC pinch-off of acoustoelectric current: (a) pinch-off with varying source-drain voltages applied at the SAW, changes are in 1 mV increments (Talyanskii et al., 1997) Copyright (1997) by The American Physical Society. (b) Pinch-off with different SAW power levels, the left most trace is 7 dBm and decrements by 0.2 dBm (Talyanskii et al., 1997) Copyright (1997) by The American Physical Society. (c) A negative anomalous acoustoelectric current for different gate voltages and SAW powers; f = 1007.426 MHz, V_{ds} = 0 V, T = 1.7 K, (Song et al., 2010)

Fig. 10 shows the oscillations of the acoustoelectric current as it is being driven through a QPC (orange trace) as it approaches pinch-off. It can be seen that the step like features observed in Fig. 9 are have been replaced by oscillations. These oscillations are negative, or on the lower cycle, when the current from the source-drain bias is flat or non-changing. We then see that as the current starts to decrease the acoustoelectric current has a positive value, or is on the upper cycle of the oscillation. The inset graph of Fig. 10 shows the entire sweep of the QPC gate voltage. As one conduction channel pinches off at the V_g = -0.65 V we see that there is a large, nearly single, oscillation in the acoustoelectric current. Since SAWs are

very sensitive to 2DEGs we get what seems to be an amplified signal when compared to a source-drain bias. This can be used to identify information that may otherwise have been too weak or nearly washed out from thermal effects.

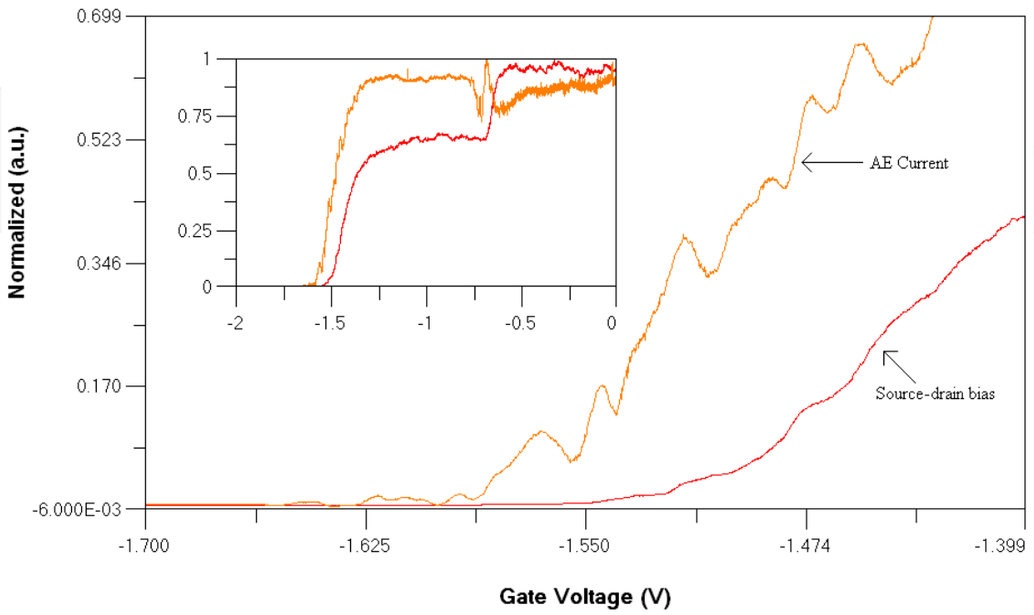

Fig. 10. Acoustoelectric current oscillations as the QPC nears pinch-off. The data plot has been normalized to show the relationship between the acoustoelectric current oscillations (orange trace) and the pinch-off when using a voltage bias across the source-drain electrodes (red trace). The acoustoelectric current trace has been normalized to -8.832 nA and the source-drain bias trace has been normalized to 4.692 nA. Measurements were taken at 4.2 K with the sample shown in Fig. 7. Inset plot shows entire gate voltage sweep range

4.3 Population and Depopulation of Quantum Dots

SAWs have been used widely as a mechanism to control the population and depopulation of QDs and DQDs. The high speed, or frequency, of operation combined with quantized current production make SAWs suitable for use with quantum systems. In a traditional QD system the gate and source-drain voltages are changed to allow single electron population and depopulation. This has several drawbacks; one being it is hard to decouple the dot from the surrounding environment due to the precise control of the voltages. There is always some noise either in the system or from the electronics. Another problem is if one gate is changed then the others must be changed to ensure a constant electron count in each dot, if applicable.

A SAW can be used as an alternative and has gotten more attention lately for the use in a QD or DQD system. The biggest reason for the attention is that SAWs can be used to interact with QD systems at much higher frequencies then what has been previously achieved by pulsing the gate electrodes. Since the acoustoelectric current can be well defined a QD system can use very high gate voltages to ensure no leakage current. We will take a look at the work done in Kataoka et al., 2007. This work describes very well the use of SAWs as a way to populate and depopulate a QD.

When the QD needs to be populated, the center plunger gate voltage value is lowered; causing the Fermi energy to lower below the Fermi energy of the surrounding 2DEG. The gate electrodes are still held at a high voltage value so the electrons cannot tunnel in or out of the QD, see Fig. 11e. The IDT is pulsed and as the SAW enters the QD region it changes the tunneling barrier created by the electrodes. The barrier is changed just enough that a single electron can tunnel into the dot, this is population; see Figs. 11a-b. The IDT is pulsed many times since the tunneling barrier is so high that the additional pulses are needed to increase the tunneling probability of the electron.

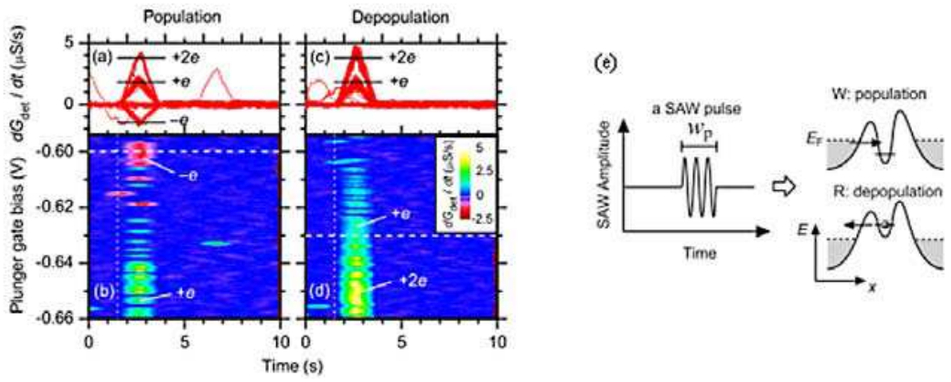

Fig. 11. Results from the paper Kataoka et al., 2007, Copyright (2007) by The American Physical Society. (a) and (b) The population of the QD, the –e line is an electron entering the dot. (c) and (d) Depopulation of the QD. (e) Schematic of SAW for population and depopulation of the QD

Likewise, as shown in Figs. 11c-d, the QD is depopulated by a similar mechanism. Here the plunger gate voltage is raised, made to be more negative, which causes the Fermi energy of the QD to be raised in comparison to the 2DEG Fermi energy outside of the dot, Fig. 11e. At this time the IDT is pulsed and the SAW enters the QD region. The SAW alters the tunneling barrier created by the gate electrodes when the potential of the SAW is superimposed onto the barrier, see Eq. 5. When the barrier is raised nothing happens since this will simply ensure the electron stays in the system, but when the negative cycle of the SAW superimposes with the barrier it decreases it which causes the electron to tunnel out.
This method of operation has proven, quite nicely, that SAWs and high potential QPCs offer a more robust method of single electron population and depopulation. As shown in Figs. 11a-d the QD can maintain the electron confinement for a long period of time which can be difficult in a traditional setup due to noise reduction of the measurement electronics. The IDTs can be accessed from an outside system such as an antenna, for example, and interact with the QD allowing the system another degree of freedom from the traditional closed electronics. However, this may come at the cost of additional noise reduction equipment and filtering.

5. Conclusion

This chapter has shown all of the basic properties and uses of SAWs in nano-structures and nano-systems. The reader is shown the parameters required for fabrication, theory of operation, real results, and application. The use of SAWs is quite limitless in the area of

NEMS. As people continue to refine the research through experiment and by continuing to add to the theory more applications will emerge.

6. Acknowledgment

We like to thank the National Science Foundation for support under a NIRT grant (No. ECCS-0708759) and the Air Force Office for Scientific Research for support under a MURI grant (No. FA9550-08-1-0337).

7. References

Barnes, C. H. W., Shilton, J. M., & Robinson, A. M. (2000). Quantum computing using electrons trapped by surface acoustic waves. *Physical Review B*, Vol. 62, No. 12, (September 2000), pp. 8410-8419, ISSN 0163-1829

Beil, F. W., Wixforth, A., Wegscheider, W., Schuh, D., Bichler, M., & Blick, R. H. (2008). Shock Waves in Nanomechanical Resonators. *Physical Review Letters*, Vol. 100, No. 2, (January 2008), pp. 026801 1-4, ISSN 0031-9007

Campbell, C. (1998). *Surface Acoustic Wave Devices for Mobile and Wireless Communications*, Academic Press, Inc, ISBN 0-12-157340-0, San Diego, CA, USA

Kataoka, M., Schneble, R. J., Thorn, A. L., Barnes, C. H. W., Ford, C. J. B., Anderson, D., Jones, G. A. C., Farrer, I., Ritchie, D. A., & Pepper, M. (2007). Single-Electron Population and Depopulation of an Isolated Quantum Dot Using a Surface-Acoustic-Wave Pulse. *Physical Review Letters*, Vol. 98, No. 4, (January 2007), pp. 46801-1 – 46801-4, ISSN 0031-9007

Kuok, M., Ng, S. C., & Zhang, V. L. (2001). Angular dispersion of surface acoustic waves on (001), (110), and (111) GaAs. *Journal of Applied Physics*, Vol. 89, No. 12, (June 2001), pp. 7899-7902, ISSN 0021-8979

Maaø, F. A. & Galperin, Y. (1997). Acoustoelectric effects in quantum constrictions. *Physical Review B*, Vol. 56, No. 7, (August 1997), pp. 4028-4036, ISSN 0163-1829

Salmon, V. (1946). A New Family of Horns. *Jounal of the Acoustical Society of America*, Vol. 17, No. 3, (January 1946), pp. 212-218, ISSN 0001-4966

Shilton, J. M., Mace, D. R., Talyanskii, V. I., Galperin, Y., Simmons, M. Y., Pepper, M., & Ritchie, D. A. (1996). On the acoustoelectric current in a one-dimensional channel. *Journal of Condensed Matter Physics*, Vol. 8, (March 1996), pp. L337-L343, ISSN 0953-8984

Song, L., Chen, S. W., He, J. H., Zhang, C. Y., Lu, C., & Gao, J. (2010). The anomalous negative acoustoelectric current in single-electron transport. *Solid State Communications*, Vol. 150, (2010), pp. 292-296, ISSN 0038-1098

Talyanskii, V. I., Shilton, J. M., Pepper, M., Smith, C. G., Ford, C. J. B., Linfield, E. H., Ritchie, D. A., & Jones, G. A. C. (1997). Single-electron transport in a one-dimensional channel by high-frequency surface acoustic waves. *Physical Review B*, Vol. 56, No. 23, (December 1997), pp. 15180-15184, ISSN 0163-1829

Wixforth, A., Scriba, J., Wassermeier, M., Kothaus, J. P., Weimann, G., & Schlapp, W. (1989). Surface acoustic waves on GaAs/$Al_xGa_{1-x}As$ heterostructures. *Physical Review B*, Vol. 40, No. 11, (October 1989), pp. 7874-7887

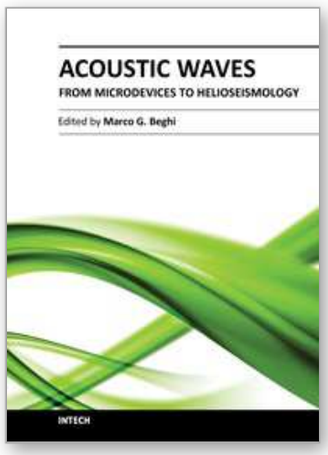

Acoustic Waves - From Microdevices to Helioseismology

Edited by Prof. Marco G. Beghi

ISBN 978-953-307-572-3
Hard cover, 652 pages
Publisher InTech
Published online 14, November, 2011
Published in print edition November, 2011

The concept of acoustic wave is a pervasive one, which emerges in any type of medium, from solids to plasmas, at length and time scales ranging from sub-micrometric layers in microdevices to seismic waves in the Sun's interior. This book presents several aspects of the active research ongoing in this field. Theoretical efforts are leading to a deeper understanding of phenomena, also in complicated environments like the solar surface boundary. Acoustic waves are a flexible probe to investigate the properties of very different systems, from thin inorganic layers to ripening cheese to biological systems. Acoustic waves are also a tool to manipulate matter, from the delicate evaporation of biomolecules to be analysed, to the phase transitions induced by intense shock waves. And a whole class of widespread microdevices, including filters and sensors, is based on the behaviour of acoustic waves propagating in thin layers. The search for better performances is driving to new materials for these devices, and to more refined tools for their analysis.

How to reference

In order to correctly reference this scholarly work, feel free to copy and paste the following:

Dustin J. Kreft and Robert H. Blick (2011). Surface Acoustic Waves and Nano–Electromechanical Systems, Acoustic Waves - From Microdevices to Helioseismology, Prof. Marco G. Beghi (Ed.), ISBN: 978-953-307-572-3, InTech, Available from: http://www.intechopen.com/books/acoustic-waves-from-microdevices-to-helioseismology/surface-acoustic-waves-and-nano-electromechanical-systems

INTECH
open science | open minds

InTech Europe
University Campus STeP Ri
Slavka Krautzeka 83/A
51000 Rijeka, Croatia
Phone: +385 (51) 770 447
Fax: +385 (51) 686 166
www.intechopen.com

InTech China
Unit 405, Office Block, Hotel Equatorial Shanghai
No.65, Yan An Road (West), Shanghai, 200040, China
中国上海市延安西路65号上海国际贵都大饭店办公楼405单元
Phone: +86-21-62489820
Fax: +86-21-62489821

IntechOpen